Journal of Materials Chemistry A

PAPER

View Article Online
View Journal | View Issue

Cite this: J. Mater. Chem. A, 2015, 3, 8324

In operando morphology investigation of inverted bulk heterojunction organic solar cells by GISAXS

Weijia Wang,[a] Christoph J. Schaffer,[a] Lin Song,[a] Volker Körstgens,[a] Stephan Pröller,[ab] Efi Dwi Indari,[a] Tianyi Wang,[a] Amr Abdelsamie,[a] Sigrid Bernstorff[c] and Peter Müller-Buschbaum*[a]

Received 10th February 2015
Accepted 11th March 2015

DOI: 10.1039/c5ta01109d

www.rsc.org/MaterialsA

Highly stable poly(3-hexylthiophene-2,5-diyl) (P3HT) : phenyl-C61-butyric acid methyl ester (PCBM) bulk heterojunction solar cells are fabricated by using an inverted geometry. The direct correlation between the morphology of the active layer and the device performance during continuous operation under illumination is revealed by *in operando* grazing incidence small angle X-ray scattering (GISAXS) and *I*–*V* measurements. Other than in devices with normal geometry, it is found that the P3HT : PCBM active layer shows a stable morphology during early operation times, which leads to an improved stability of the short circuit current and accordingly the power conversion efficiency of the inverted solar cell. Furthermore, the inverted P3HT : PCBM solar cells are long-term stable without encapsulation if they are stored under ambient dark conditions. It reveals that the power conversion efficiency preserves around 88% of the initial value after more than 150 days.

Introduction

Over the last few decades, organic solar cells have been intensively investigated since they allow for easy power generation even where the use of conventional inorganic photovoltaic devices is not feasible. Organic solar cells can be made from branches of organic semiconductors, which provide them unique properties.[1–4] The main advantages associated with organic solar cells are low weight, mechanical flexibility, less energy consumption and manufacturing costs as compared to other photovoltaic technologies, and a wide variety of production methods including roll-to-roll printing techniques.[5–8] This promising prospect of organic solar cells encourages massive research on developing new organic material systems or designing new solar cell architectures to make their photovoltaic performance comparable to traditional inorganic solar cells based on silicon.[9] Remarkable progress has been made to improve the power conversion efficiency (PCE) of organic solar cells. By utilizing low band gap polymers, the PCE of the polymer-fullerene bulk heterojunction (BHJ) solar cell has exceeded 8–10%.[10–12] Recently, a PCE around 10% has been achieved through using an inverted geometry.[13] Although high performances are achieved, the short lifetimes of organic solar panels still impede their commercialization.[14–17] Thus, improvements to achieve long term stability are highly desirable, which in turn will become easier with a better understanding of the degradation processes.

Poly(3-hexylthiophene-2,5-diyl) (P3HT) : phenyl-C61-butyric acid methyl ester (PCBM) BHJ organic solar cells with a standard geometry is the most investigated system today, which is frequently used to investigate the structure-property relationships.[18–23] In order to improve the stability of these devices, many of the processes leading to degradation have been identified. Thus, some general mechanisms of device degradation were proposed, including oxidation of the conjugated polymer and the top electrode, diffusion of water and oxygen molecules into solar cells, erosion of bottom electrodes made from indium tin oxide (ITO) and physical degradation such as the morphological degradation of the P3HT : PCBM active layer.[14,24–27] By utilizing optimized encapsulation, several of these processes can be retarded or suppressed, which gives a significant increase in the lifetime of the solar cells.[28] Moreover, it was demonstrated that an efficient approach to minimize the degradation process is to adopt the construction of P3HT : PCBM solar cells in the so-called inverted geometry.[29,30] Compared to the standard geometry, charge carriers are extracted at the opposite electrodes, where positive charge carriers flow from P3HT to the bottom electrode and negative charge carriers transfer to the top electrode. Hau *et al.* demonstrated an inverted P3HT : PCBM solar cell using zinc oxide (ZnO) as a hole blocking layer retaining more than 80% efficiency over 40 days and attributed this long term stability to the less air sensitive high work function metal (silver) as the top

[a]Technische Universität München, Physik-Department, Lehrstuhl für Funktionelle Materialien, James-Franck-Str. 1, 85748 Garching, Germany. E-mail: muellerb@ph.tum.de; Fax: +49-89-289-12473; Tel: +49-89-289-12451

[b]Technische Universität München, Munich School of Engineering, Herzig Group, Lichtenbergstr. 4, 85748 Garching, Germany

[c]Elettra – Sincrotrone Trieste S.C.p.A., Strada Statale 14 – km 163.5 in AREA Science Park, Basovizza, 34149 Trieste, Italy

electrodes.[29] Inverted solar cells with a ZnO/poly(ethylene glycol) (PEG) hybrid hole blocking layer, which was prepared *via* a low temperature route, also showed a relatively low level of 23% degradation of the PCE after 14 days.[31]

Among the work related to inverted P3HT : PCBM BHJ solar cells, most work has been dedicated to the improvement of solar cell performance or extending the lifetime. Only a few general statements were proposed to explain the stability benefits from the inverted geometry. One of the viewpoints is that the replacement of the acidic poly(3,4-ethylenedioxythiophene) : poly(styrenesulfonate) (PEDOT : PSS) layer with a compact titanium dioxide (TiO_2) or ZnO layer on ITO can help to overcome the erosion of the bottom electrodes.[32,33] Additionally, the P3HT : PCBM active layer can be protected from degradation induced by ultraviolet (UV) light illumination as the compact hole blocking layer (TiO_2 or ZnO) absorbs UV light before reaching the active layer.[34] The general build-up in the inverted geometry implies that the active layer is sandwiched between two blocking layers, which could reduce polymer oxidation caused by contact with air. All these statements are based on the minimization of the chemical degradation. However, to our knowledge, detailed fundamental understanding from the perspective of the physical stability, such as the stability of the active layer morphology, is still unclear. For devices with normal geometry, our previous work has already shown that the nanomorphology of the photoactive P3HT : PCBM layer is not stable.[14] We observed a morphological degradation, where smaller domains in the active layer vanished and larger ones grew. These changes in the nanomorphology caused a reduction of the effective area for electrical power conversion and accordingly the degradation of the solar cell's short circuit current (J_{SC}), which plays the most important role in the degradation of standard P3HT : PCBM solar cells.[14] In the present work, the direct correlation between the morphology and device performance of inverted P3HT : PCBM BHJ solar cells is investigated during operation for the first time.

In order to probe the morphological evolution of the P3HT : PCBM inverted solar cells during operation under continuous air-mass 1.5 global (AM1.5G) sunlight illumination, *in operando* grazing incidence small angle X-ray scattering (GISAXS) is used. GISAXS is an advanced scattering technique, which provides information about the nanomorphology of thin film samples.[35,36] By selecting a suitable sample-detector distance (SDD), structures on length scales ranging from several nanometers up to a micrometer can be addressed.[4,37,38] Meanwhile, the *in situ* current–voltage (*I–V*) characteristics of the inverted P3HT : PCBM solar cell are also characterized under the same conditions. In order to compare with the previous work on standard geometry devices, the same experimental design was used during *in operando* GISAXS and *I–V* measurements, which minimizes the degradation from oxygen and moisture.[14] Through *in operando* GISAXS and *I–V* measurements on inverted devices during continuous operation, it is observed that the morphology of the solar cell is stable over time and the PCE of the solar cell is preserved to 75% after 240 minutes. By comparing the stability of photovoltaic parameters (J_{SC}; open circuit voltage (V_{OC}) and fill factor (FF)) in standard and inverted P3HT : PCBM solar cells during operation, it is clear that the stability of J_{SC} is the most enhanced parameter, while the others stay similar to the ones in standard devices. The photovoltaic parameters of the standard P3HT : PCBM solar cell were reported in our previous work.[14] Thus, the improved stability of the inverted P3HT : PCBM solar cell is attributed to the stabilization of J_{SC}. As a consequence, the improved stability of the P3HT : PCBM inverted solar cells is mainly attributed to a stable morphology of the active layer as we demonstrate in the present investigation. Additionally, the long term stability of the P3HT : PCBM inverted solar cells without encapsulation, stored under dark, ambient conditions, is examined by measuring the *I–V* characteristics periodically. If not operated continuously, the solar cells show 88% PCE preserved after more than 150 days. Therefore, to our knowledge, the probed inverted P3HT : PCBM solar cells are among the most stable reported P3HT : PCBM solar cells.

Experimental section

Materials

Poly(3-hexylthiophene-2,5-diyl) (P3HT) was purchased from Rieke Metals, Inc with an average molecular weight M_w of 50 kg mol^{-1}. Phenyl-C61-butyric acid methyl ester (PCBM) was purchased from Nano-C. Poly(3,4-ethylenedioxythiophene) : poly(styrenesulfonate) (PEDOT : PSS) solution (PH1000) was purchased from Ossila. The solvents (chlorobenzene and isopropanol), from Carl Roth, were used as supplied, as were the active materials. Solar cells were fabricated on fluorine-doped tin oxide (FTO) substrates, which were purchased from Solaronix with the size of 2.2 × 2.2 cm^2.

Sample preparation

The FTO was partly removed from the substrates by chemical etching and used as a bottom electrode for the inverted solar cells. The substrates were then cleaned consecutively with Alconox® solution, ethanol, acetone and isopropanol in an ultrasonic bath and treated with oxygen plasma. The hole blocking layer composed of a compact titanium dioxide film was prepared with the method reported in the work of Yu *et al.*[39] To prepare the P3HT : PCBM solution, P3HT was first dissolved in chlorobenzene until completely dissolved and then added to dry PCBM. Solutions were stirred overnight. The concentration of the blends was 24 mg mL^{-1} with a polymer : fullerene ratio of 1 : 1. The solution was spin-coated on the titanium dioxide layer with a rotation speed of 2000 rpm for 30 seconds. As reported by Weickert *et al.*, diluted PEDOT : PSS solution is suitable for preparing the electron blocking layer by spray-coating.[40] Thus, the PEDOT : PSS solution as obtained was filtered by a PVDF filter (with the pore size of 0.45 μm) and then diluted with isopropanol at the ratio of 1 : 10. The diluted PEDOT : PSS solution was spray-coated for 15 seconds on the P3HT : PCBM layer by a commercial airbrush gun (Harder & Steenbeck) with 5 cm distance normal to the sample surface. Oil-free nitrogen with a pressure of 1 bar was used as the carrier gas. Afterwards, the sample was spin-dried with a rotation speed of 2000 rpm for

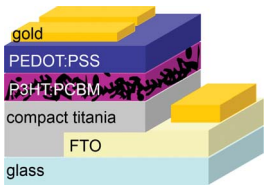

Fig. 1 Scheme of the inverted P3HT : PCBM solar cell layer structure used in the present investigation.

60 seconds. Gold electrodes were deposited on top of the PEDOT : PSS layer by physical vapor deposition, followed by thermal annealing at 140 °C for 10 min in a closed environment with a constant nitrogen flow. The scheme of the final device layer structure is shown in Fig. 1 to illustrate the inverted geometry.

In operando grazing incidence small angle X-ray scattering (GISAXS)

The *in operando* GISAXS experiments were performed at the Austrian SAXS beamline of the Elettra synchrotron source in Trieste, Italy. The X-ray wavelength was 0.154 nm. The sample-detector distance was 1776 mm. An incident angle of 0.53° was selected, which is above the critical angle of all polymers involved in the solar cell, TiO_2 and FTO. The sample was fully penetrated at this incident angle, therefore both surface and inner film structures were probed. The set-up employed for mounting the solar cell for *in operando* GISAXS measurements followed the one described in our previous work.[14] Thus, the solar cell was mounted in an evacuated chamber, which enabled simultaneous *I–V* measurements and GISAXS characterization.[14] Since the scattering signal of the gold electrode outweighed the signal with the structural evolution of the P3HT : PCBM layer, the scattering data were collected at three positions close to the gold electrode.

The exposure time of each single measurement was 40 s. No X-ray irradiation damage or influence on the *I–V* measurements was observed. The solar cell was operated continuously under illumination using a 150 W Xenon short arc lamp (Perkin Elmer PX5) employing a constant intensity of 100 mW cm^{-2}. The GISAXS data were obtained before illumination, denoted as 0 min, and then after 3 min, 10 min, 15 min, 30 min, 60 min, 120 min, 180 min and 240 min. In order to analyze the horizontal line cuts, a model in the framework of the distorted wave Born approximation (DWBA) and the local monodisperse approximation (LMA) was applied, which is based on contributions from three substructures each described by a form factor (average structure size) and a structure factor (average center-to-center distance) according to a 1d paracrystal as proposed by Hosemann *et al.*[41]

The current–voltage characteristics of the inverted solar cell were recorded constantly each 16 seconds using a source meter Keithley 2400 for 240 min. A silicon based reference solar cell was used to calibrate the applied AM1.5 conditions. By using a calibrated microscope, the solar cell pixel size was measured.

Long term stability measurements

The inverted P3HT : PCBM solar cells were stored in air under ambient conditions without any encapsulation in the dark. The efficiency measured directly after the solar cell preparation was denoted as the initial efficiency. Later, the long term stability was investigated by measuring *I–V* characteristics periodically.

Results and discussion

Morphology evolution

The inverted P3HT : PCBM solar cells are built following a layered architecture of FTO/TiO_2/P3HT : PCBM/PEDOT : PSS/gold without additional encapsulation (see Fig. 1). As is known, the nanomorphology of the photoactive layer is crucial for the solar cell performance.[42,43] To investigate the nanomorphology of the BHJ layer evolution during the first 240 min of operation under solar illumination (100 mW cm^{-2}), *in operando* GISAXS is performed. It has been proven to be a powerful technique to probe the morphological degradation on a nanometer scale in polymer solar cells.[14] Therefore, *in operando* GISAXS measurements on the P3HT : PCBM inverted solar cell are carried out to track the evolution of the morphology. In order to compare with our previous work about the morphological evolution of P3HT : PCBM in a standard geometry, the inverted device was installed in the same chamber that was evacuated to minimize the influence of oxygen and moisture. Through excluding the different influence from these two main factors on standard and inverted solar cell degradation, the investigation is mainly focused on the degradation due to changes of the nanomorphology of the BHJ layer.

The two dimensional (2D) GISAXS data are taken before illumination (denoted as 0 min) and after 3 min, 10 min, 15 min, 30 min, 60 min, 120 min, 180 min and 240 min of illumination. The initial 2D GISAXS data are shown in Fig. 2 as an example. The Yoneda peaks are observed at the critical angles, which clearly display a bright region at the bottom of the 2D GISAXS pattern. Additionally, the P3HT (100) Bragg reflection is observed at the top of the pattern, which shows a spot-like feature. It reveals that P3HT crystallites exist in the photoactive layer. Within all *in operando* GISAXS measurements, the GISAXS patterns have not changed significantly.

In order to obtain the structural information normal to the film, surface vertical line cuts are extracted from the 2D GISAXS data measured before illumination (0 min) and after 3 min, 10 min, 15 min, 30 min, 60 min, 120 min, 180 min and 240 min illumination at the position $q_y = 0$ and plotted in Fig. 3a. For improved statistics three data points are averaged in the presentation. To clearly visualize the evolution of the vertical line cuts as a function of illumination time, all curves are plotted on top of each other. The Yoneda peak of P3HT is visible for all the vertical line cuts, located at around $q_z = 0.48$ nm^{-1}, and denoted by an arrow in the inset of Fig. 3a. The Yoneda peak belonging to FTO ($q_z = 0.63$ nm^{-1}) is not visible as it is superimposed by that of the P3HT : PCBM blend film. Since the vertical line cuts show identical features (Fig. 3a), we can conclude that the vertical film composition is stable. Besides,

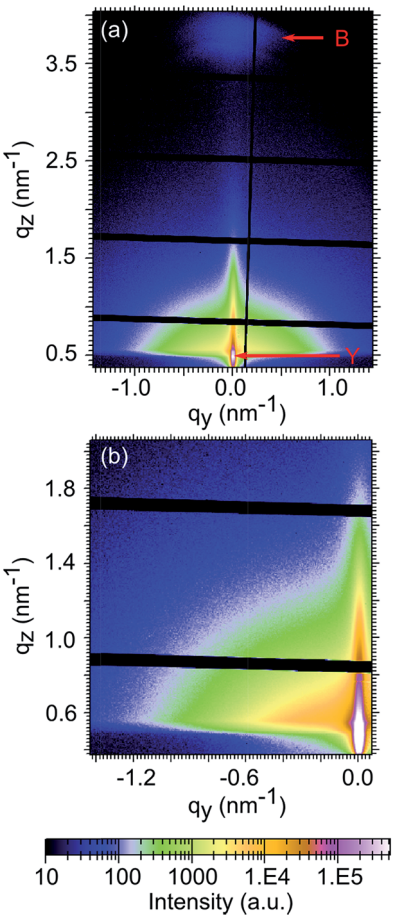

Fig. 2 (a) Initial 2D GISAXS data of a P3HT : PCBM inverted solar cell before illumination with well pronounced Yoneda peak (Y) and (100) Bragg peak (B). (b) Zoom into the Yoneda region of the 2D GISAXS data.

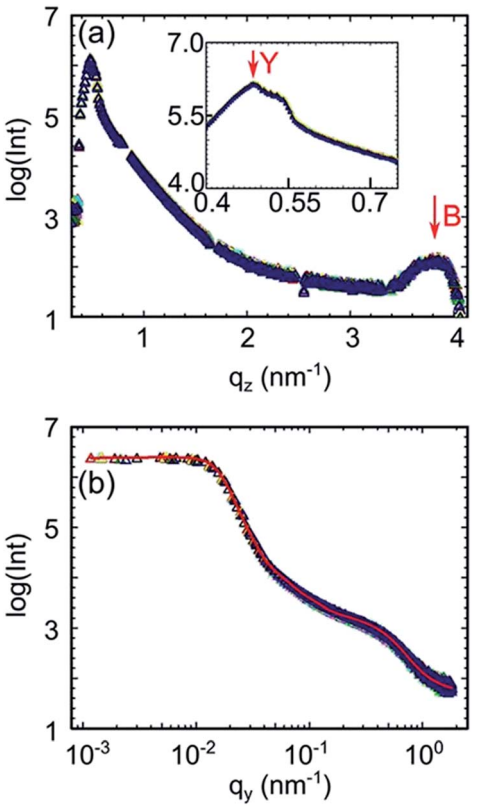

Fig. 3 (a) Vertical line cuts and (b) horizontal line cuts (triangles) and corresponding fits (solid red line) of the 2D GISAXS data measured before the illumination (0 min) and after 3 min, 10 min, 15 min, 30 min, 60 min, 120 min, 180 min and 240 min. To visualize the absence of changes in the line cuts as a function of illumination time, all cuts are plotted on top of each other. Different colors of the symbols denote different illumination times. In (a) three data points are averaged for better visualization and a zoom into the Yoneda region of the vertical line cuts is shown as the inset.

there is no indication for molecular diffusion arising during 240 min operating time under illumination since the Yoneda peak region, which reveals the material composition, remains unchanged.[44]

Additionally, the P3HT (100) Bragg reflection peak is visible (Fig. 3a), located at $q_z = 3.75$ nm^{-1}, which corresponds to a lattice constant of 1.68 nm. This value is in good agreement with previous investigations.[43,45–47] The FWHM value of 0.63 ± 0.05 is obtained by fitting this Bragg peak and corresponds to the correlation length of 10 ± 0.8 nm in the (100) direction, as determined by using the Scherrer equation. The (100) peak does not change with illumination time, indicating that the P3HT crystalline order is stable with respect to the edge-on orientation in the inverted polymer solar cell during 240 min operating time under solar illumination.

Lateral structure information can be obtained by performing horizontal line cuts to the 2D GISAXS data.[37] Hereby, the material shows the most pronounced scattering intensity at its Yoneda peak position.[48] Since the morphology of the photoactive P3HT : PCBM layer plays the most important role in photovoltaic performance of the solar cell,[49] all the horizontal line cuts are applied at the critical angle of P3HT (around 0.16°) to emphasize on this material. Similar to the way of displaying all the vertical line cuts, the horizontal line cuts of the *in operando* study are also plotted on top of each other, as shown in Fig. 3b. It is noticed that all these curves completely overlap, which suggests that the morphology of the P3HT : PCBM layer is stable during 240 min operating time under illumination. However, Schaffer *et al.* reported that P3HT domains grow with the time in a polymer solar cell with a standard geometry.[14] Compared to that, the morphology of the P3HT : PCBM layer in the inverted device is fully stabilized. This highly improved stability may be enabled by the TiO_2 layer underneath. On the one hand, less P3HT chain scission caused by UV light illumination may occur due to the absorbance of the TiO_2 layer underneath. Accordingly, the chain mobility of P3HT stays low and does not allow for structure relaxation when the chains retain their molecular weight. On the other hand, the interactions between the P3HT : PCBM film and the layer underneath also have strong influence on the morphology as described by Campoy-Quiles *et al.*[50] Zhao *et al.* also revealed that the P3HT films on conductive substrates showed significantly retarded

degradation and preservation of the chemical and morphological features as compared to P3HT films on glass substrates.[51]

The average structure sizes and the distances of P3HT can be extracted from the fitting of the horizontal line cuts. One fitting matches for all the horizontal line cuts from the *in operando* investigation, as shown in Fig. 3b. The average P3HT structure sizes of 2.5 ± 0.2, 19 ± 1 and 82 ± 4 nm can be observed, with the corresponding average distances of 45 ± 5, 180 ± 30 and 420 ± 100 nm. In summary, the morphology of the P3HT : PCBM layer and the P3HT crystalline order are both fully stable in an inverted polymer solar cell on a time scale of several hours of operation.

In situ current–voltage characterization

In the inverted polymer solar cell, the morphology of P3HT : PCBM layer is stable during the first 240 min operating time under continuous solar illumination. In order to probe the stability of the photovoltaic performance during this time the cell is investigated simultaneously in terms of *I–V* tracking. *I–V* sweeps are hereby recorded every 16 seconds during illumination. Selected *I–V* curves (at the beginning of the illumination (denoted as 0 min) and after 3 min, 10 min, 15 min, 30 min, 60 min, 120 min, 180 min and 240 min) are shown in Fig. 4, These *I–V* curves represent the state at the times when the 2D GISAXS data have been recorded. The initial one (0 min) shows an S-shaped curve, owing the smallest J_{SC} and V_{OC} as compared to all the other measurements. Then, the S-shaped curve transits towards a generally more rectangle-like curve during the operation, which suggests a self-healing process that occurs during operation. Lloyd *et al.* have observed a similar behavior in an inverted organic photovoltaic device. They have attributed this initial improvement to the evolution of the interface between the active layer and the silver electrode.[52] The *I–V* curves recorded at 3 min and at 10 min appear similar, which indicates a stable photovoltaic performance of the device in this stage of operation. After 10 min of illumination, the *I–V* curves decay slowly with the illumination time, showing a continuously decreasing J_{SC} and V_{OC}.

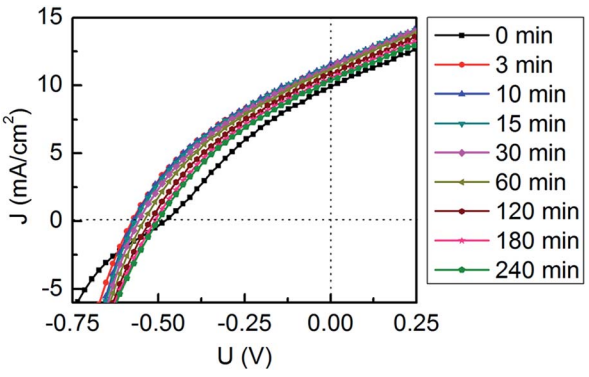

Fig. 4 *I–V* curves of the P3HT : PCBM inverted solar cell as function of illumination time. *I–V* curves are recorded constantly every 16 seconds under continuous illumination for 240 min. The selected curves are matching the times of the *in operando* GISAXS study as indicated by the color code.

The photovoltaic parameters of J_{SC}, V_{OC}, FF and PCE are extracted from each *I–V* measurement and plotted as a function of illumination time in Fig. 5. For improved statistics five data points are averaged in this presentation. All the parameters increase dramatically during the first few minutes and then stay nearly constant until roughly 10 min. After that, a slow but continuous decay of all the parameters follows. The decay of PCE results from the degradation of all three other photovoltaic parameters. Compared to the standard device,[14] V_{OC} decays similarly. A potential reason can be the change in temperature, as it is known that the temperature has a strong influence on V_{OC}. During the measurements, the temperature on the device was increased by only 10 °C, which still might explain the observed decay of V_{OC}. Guo *et al.* had also observed a voltage decrease with increasing temperature.[23] They attributed the reason to the degradation of the photoactive layer caused by photochemical reactions in polymer.

In contrast, the FF decays extremely slowly, thereby showing the same trend as observed in a standard device.[14] However, since the absolute FF values are quite small, a stronger decay might occur in the device, which exhibit higher FF values. In a standard geometry device, the morphological transition of the P3HT : PCBM layer can fully explain the degradation of J_{SC}.[14] In contrast, in this work J_{SC} still slowly decreases even with a stable P3HT : PCBM layer morphology, which might hint to some fundamental differences between the standard and inverted geometry.

In order to clearly illustrate the contributions of J_{SC}, V_{OC} and FF to the decay of PCE, all the parameters are normalized to their maximum values and depicted in Fig. 6. As compared to a standard P3HT : PCBM solar cell,[14] PCE and J_{SC} show the most improved stability in the inverted geometry while FF and V_{OC} exhibit a similar decay behavior. The J_{SC} and PCE are preserved above 90% and 75% after 240 min of operation, whereas for cells in standard geometry around 80% and 65% were reported after 240 min of operation.[14] It implies that the improvement of the PCE stability mainly benefits from the stabilization of J_{SC}.

Related to the above investigation on the morphology *via in operando* GISAXS measurements, it is inferred that the strongly improved stability of J_{SC} is caused by a stable morphology of the active layer of P3HT : PCBM in an inverted geometry. Similarly, Schaffer *et al.* concluded that the change in the nano-morphology of P3HT : PCBM layer is an extremely important pathway of the J_{SC} decay.[14] Based on our investigations, we conclude that the stabilized P3HT : PCBM active layer contributes to a highly improved stability of J_{SC}, while it has no prominent influence on the temporal evolution of FF and V_{OC}. Accordingly, the stability of PCE is improved as compared to a standard solar cell.

Furthermore, the long term stability of inverted P3HT : PCBM solar cells was examined. An inverted device was kept in air under ambient conditions in the dark. The *I–V* measurements were carried out periodically. The PCE of the inverted device preserves 88% compared to its maximum value after more than 150 days. In summary, a significant improvement in the long-term stability of the device is obtained by using

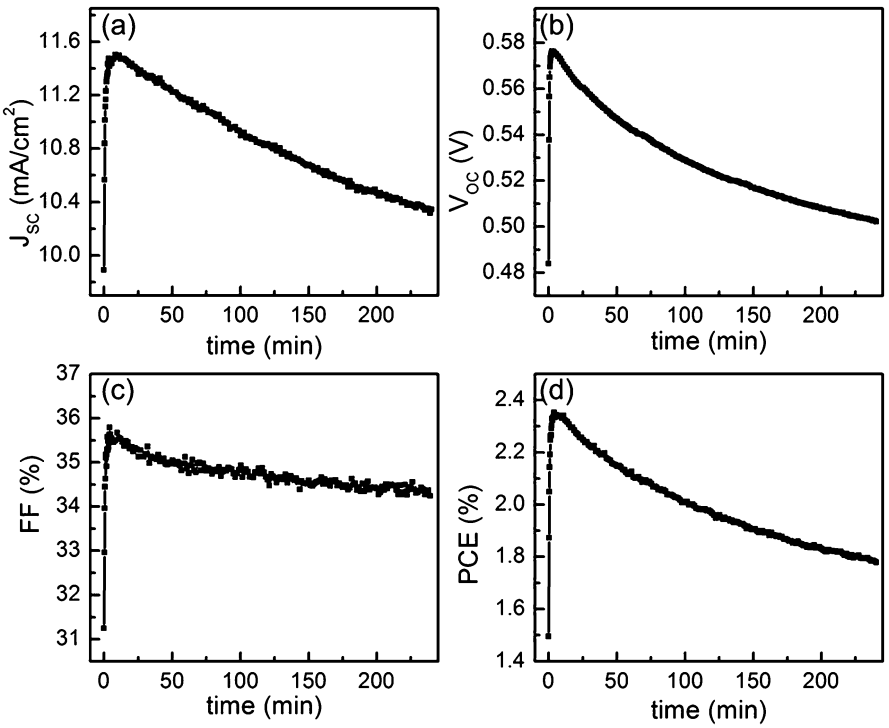

Fig. 5 Time evolution of the photovoltaic characteristics of (a) J_{SC}, (b) V_{OC}, (c) FF and (d) PCE of the P3HT : PCBM inverted solar cell. The devices have been measured constantly every 16 seconds under continuous illumination for 240 min during the *in operando* GISAXS study. Five data points are averaged for better visualization.

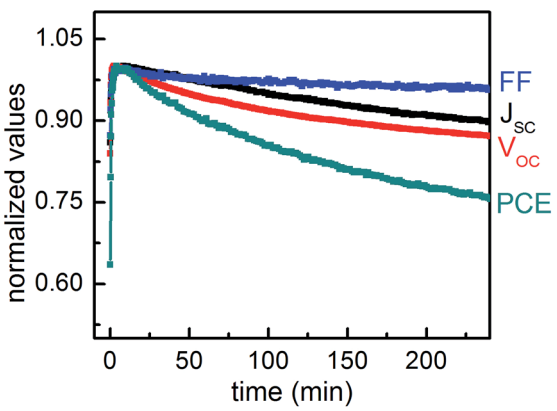

Fig. 6 Time evolution of the normalized photovoltaic characteristics (J_{SC}, V_{OC}, FF and PCE) of the P3HT : PCBM inverted solar cell probed during the *in operando* GISAXS study. J_{SC}, V_{OC}, FF and PCE are normalized to their maximum values. Five data points are averaged for better visualization.

an inverted geometry, also when stored in air under ambient conditions.

Conclusion

In this work we demonstrate a highly stable P3HT : PCBM BHJ solar cell in an inverted geometry. To understand the correlation between the morphology and the device performance during continuous operation under illumination, *in operando* GISAXS and *I–V* characteristic measurements are performed. Around 75% of PCE is preserved after 240 min continuous operation, which is higher than that observed in a standard solar cell. This improvement results from an increased stability of J_{SC}. A stable morphology of the P3HT : PCBM layer, which benefits from the inverted geometry of the device, is revealed by the *in operando* GISAXS measurements. This stabilization of the P3HT : PCBM layer is directly correlated with an improved stability of J_{SC} of the solar cell for the first time. Moreover, no prominent influence is observed on the decay behavior of the FF and V_{OC}. Moreover, the inverted solar cell is long term stable, when it is kept in air under dark, ambient conditions and measured periodically. Surprisingly, the PCE of the inverted device is maintained at around 88% after more than 150 days compared to its maximum value if not measured continuously. Thus, the present investigation shows that proper tuning of the stability of the morphology of the active layer, such as using an inverted geometry, can contribute to highly stable polymer solar cells.

Acknowledgements

This work is financially supported by TUM.solar in the frame of the Bavarian Collaborative Research Project “Solar technologies go Hybrid" (SolTec), the GreenTech Initiative (Interface Science for Photovoltaics - ISPV) of the EuroTech Universities, the German Research Foundation (DFG) in the “SPP1355: Elementary processes of organic photovoltaics”, and the Nanosystems Initiative Munich (NIM). W.W. and L.S. thank the China

Scholarship Council (CSC) and E.D.I., T.W. and A.A. thank the Erasmus Mundus "MaMaSELF" program. Funding by the Bavarian State Ministry of Education, Science and the Arts *via* the International Graduate School "Materials Science of Complex Interfaces" (CompInt) is acknowledged by C.J.S. and *via* the project "Energy Valley Bavaria" by V.K. and S.P. We thank D. Magerl for introducing the fitting model for horizontal line cuts in 2D GISAXS data.

Notes and references

1 S. B. Darling and F. You, *RSC Adv.*, 2013, **3**, 17633.
2 C. J. Brabec, N. Serdar Sariciftci and J. C. Hummelen, *Adv. Funct. Mater.*, 2001, **11**, 15.
3 M. Kaltenbrunner, M. S. White, E. D. Głowacki, T. Sekitani, T. Someya, N. Serdar Sariciftci and S. Bauer, *Nat. Commun.*, 2012, **3**, 770.
4 M. A. Ruderer and P. Müller-Buschbaum, *Soft Matter*, 2011, **7**, 5482.
5 B. C. Thompson and J. M. J. Fréchet, *Angew. Chem., Int. Ed.*, 2008, **47**, 58.
6 T. Ameri, T. G. Dennler, C. Lungenschmied and C. J. Brabec, *Energy Environ. Sci.*, 2009, **2**, 347.
7 M. C. Scharber and N. S. Sariciftci, *Prog. Polym. Sci.*, 2013, **38**, 1929.
8 F. Nickel, T. Haas, E. Wegner, D. Bahro, S. Salehin, O. Kraft, P. A. Gruber and A. Colsmann, *Sol. Energy Mater. Sol. Cells*, 2014, **130**, 317.
9 L. Lu and L. Yu, *Sol. Adv. Mater.*, 2014, **26**, 4413.
10 Z. He, C. Zhong, X. Huang, W.-Y. Wong, H. Wu, L. Chen, S. Su and Y. Cao, *Adv. Mater.*, 2011, **23**, 4636.
11 M. A. Green, K. Emery, Y. Hishikawa, W. Warta and E. D. Dunlop, *Prog. Photovoltaics*, 2014, **22**, 701.
12 J.-D. Chen, C. Cui, Y.-Q. Li, L. Zhou, Q.-D. Ou, C. Li, Y. Li and J.-X. Tang, *Adv. Mater.*, 2015, **27**, 1035.
13 Z. He, C. Zhong, S. Su, M. Xu, H. Wu and Y. Cao, *Nat. Photon.*, 2011, **6**, 591.
14 C. J. Schaffer, C. M. Palumbiny, M. A. Niedermeier, C. Jendrzejewski, G. Santoro, S. V. Roth and P. Müller-Buschbaum, *Adv. Mater.*, 2013, **25**, 6760.
15 B. Lechêne, J. Leroy, O. Tosoni, R. de Bettignies and G. Perrier, *J. Phys. Chem. C*, 2014, **118**, 20132.
16 A. Moujoud, S. H. Oh, J. J. Hye and H. J. Kim, *Sol. Energy Mater. Sol. Cells*, 2011, **95**, 1037.
17 C. H. Peters, I. T. Sachs-Quintana, J. P. Kastrop, S. Beaupré, M. Leclerc and M. D. McGehee, *Adv. Energy Mater.*, 2011, **1**, 491.
18 R. D. Bettignies, J. Leroy, M. Firon and C. Sentein, *Synth. Met.*, 2006, **156**, 510.
19 J. A. Hauch, P. Schilinsky, S. A. Choulis, R. Childers, M. Biele and C. J. Brabec, *Sol. Energy Mater. Sol. Cells*, 2008, **92**, 727.
20 M. O. Reese, A. J. Morfa, M. S. White, N. Kopidakis, S. E. Shaheen, G. Rumbles and D. S. Ginley, *Sol. Energy Mater. Sol. Cells*, 2008, **92**, 746.
21 C. Lungenschmied, G. Dennler, H. Neugebauer, S. N. Sariciftci, M. Glatthaar, T. Meyer and A. Meyer, *Sol. Energy Mater. Sol. Cells*, 2007, **91**, 379.
22 S. Guo, M. A. Ruderer, M. Rawolle, V. Körstgens, C. Birkenstock, J. Perlich and P. Müller-Buschbaum, *ACS Appl. Mater. Interfaces*, 2013, **5**, 8581.
23 S. Guo, C. Brandt, T. Andreev, E. Metwalli, W. Wang, J. Perlich and P. Müller-Buschbaum, *ACS Appl. Mater. Interfaces*, 2014, **6**, 17902.
24 M. Jørgensen, K. Norrman and F. C. Krebs, *Sol. Energy Mater. Sol. Cells*, 2008, **92**, 686.
25 K. Norrman and F. C. Krebs, *Sol. Energy Mater. Sol. Cells*, 2006, **90**, 213.
26 B. Conings, S. Bertho, K. Vandewal, A. Senes, J. D'Haen, J. Manca and R. A. J. Janssen, *Appl. Phys. Lett.*, 2010, **96**, 163301.
27 K. Norrman, M. V. Madsen, S. A. Gevorgyan and F. C. Krebs, *J. Am. Chem. Soc.*, 2010, **132**, 16883.
28 R. Tipnis, J. Bernkopf, S. Jia, J. Krieg, S. Li, M. Storch and D. Laird, *Sol. Energy Mater. Sol. Cells*, 2009, **93**, 442.
29 S. K. Hau, H.-L. Yip, N. S. Baek, J. Zou, K. O'Malley and A. K.-Y. Jen, *Appl. Phys. Lett.*, 2008, **92**, 253301.
30 M. T. Lloyd, D. C. Olson, P. Lu, E. Fang, D. L. Moore, M. S. White, M. O. Reese, D. S. Ginley and J. W. P. Hsu, *J. Mater. Chem.*, 2009, **19**, 7638.
31 T. Hu, F. Li, K. Yuan and Y. Chen, *ACS Appl. Mater. Interfaces*, 2013, **5**, 5763.
32 L.-M. Chen, Z. Xu, Z. Hong and Y. Yang, *J. Mater. Chem.*, 2010, **20**, 2575.
33 S. Lattante, *Electronics*, 2014, **3**, 132.
34 H. Sun, J. Weickert, H. C. Hesse and L. Schmidt-Mende, *Sol. Energy Mater. Sol. Cells*, 2011, **12**, 3450.
35 G. Renaud, R. Lazzari and F. Leroy, *Surf. Sci. Rep.*, 2009, **64**, 255.
36 A. Hexemer and P. Müller-Buschbaum, *IUCrJ*, 2015, **2**, 106.
37 P. Müller-Buschbaum, *Anal. Bioanal. Chem.*, 2003, **376**, 3.
38 P. Müller-Buschbaum, *Adv. Mater.*, 2014, **26**, 7692.
39 H. Yu, S. Zhang, H. Zhao, G. Will and P. Liu, *Electrochim. Acta*, 2009, **54**, 1319.
40 J. Weickert, H. Sun, C. M. Palumbiny, H. C. Hesse and L. Schmidt-Mende, *Sol. Energy Mater. Sol. Cells*, 2010, **94**, 2371.
41 R. Hosemann, W. Vogel, D. Weick and F. J. Baltá-Calleja, *Acta Crystallogr.*, 1981, **37**, 85.
42 P. Kohn, Z. Rong, K. H. Scherer, A. Sepe, M. Sommer, P. Müller-Buschbaum, R. H. Friend, U. Steiner and S. Hüttner, *Macromolecules*, 2013, **46**, 4002.
43 M. A. Ruderer, S. Guo, R. Meier, H.-Y. Chiang, V. Körstgens, J. Wiedersich, J. Perlich, S. V. Roth and P. Müller-Buschbaum, *Adv. Funct. Mater.*, 2011, **21**, 3382.
44 Y. Yoneda, *Phys. Rev.*, 1963, **131**, 2010.
45 S. Hugger, R. Thomann, T. Heinzel and T. Thurn-Albrecht, *Colloid Polym. Sci.*, 2004, **282**, 932.
46 Z. Wu, A. Petzold, T. Henze, T. Thurn-Albrecht, R. H. Lohwasser, M. Sommer and M. Thelakkat, *Macromolecules*, 2010, **43**, 4646.
47 K. Sethuraman, S. Ochiai, K. Kojima and T. Mizutani, *Appl. Phys. Lett.*, 2008, **92**, 183302.
48 G. Renaud, R. Lazzari and F. Leroy, *Surf. Sci. Rep.*, 2009, **64**, 255.

49 D. Chirvase, J. Parisi, J. C. Hummelen and V. Dyakonov, *Nanotechnology*, 2004, **15**, 1317.
50 M. Campoy-Quiles, T. Ferenczi, T. Agostinelli, P. G. Etchegoin, Y. Kim, T. D. Anthopoulos, P. N. Stavrinou, D. D. C. Bradley and J. Nelson, *Nat. Mater.*, 2008, **7**, 158.
51 Y. Zhao, A. Sugunan, T. Schmidt, A. Fornara, M. S. Toprak and M. Muhammed, *J. Mater. Chem. A*, 2014, **2**, 13270.
52 M. T. Lloyd, C. H. Peters, A. Garcia, I. V. Kauvar, J. J. Berry, M. O. Reese, M. D. McGehee, D. S. Ginley and D. C. Olson, *Sol. Energy Mater. Sol. Cells*, 2011, **95**, 1382.